Effective Stress Law for the Permeability and Pore Volume Change of Clayey Sandstones

Fanbao Meng, Xingfu Li, Patrick Baud, Teng-fong Wong

JGR Solid Earth

RESEARCH ARTICLE
10.1029/2020JB019765

Effective Stress Law for the Permeability and Pore Volume Change of Clayey Sandstones

Fanbao Meng[1], Xingfu Li[1], Patrick Baud[2], and Teng-fong Wong[1]

[1]Earth System Science Programme, Faculty of Science, The Chinese University of Hong Kong, Hong Kong, [2]Institut de Physique du Globe de Strasbourg (UMR 7516 CNRS), Université de Strasbourg/EOST, Strasbourg, France

Key Points:
- Our study is the first integrated investigation of the effective stress behaviors for permeability and pore volume change in sandstones
- The presence of microcracks will influence the effective stress behavior, decreasing the effective stress coefficient for permeability
- We propose a dual equivalent-channel model to resolve apparent discrepancies between experimental data and existing models

Correspondence to:
F. Meng,
quanquanmfb@163.com

Citation:
Meng, F., Li, X., Baud, P., & Wong, T. (2020). Effective stress law for the permeability and pore volume change of clayey sandstones. *Journal of Geophysical Research: Solid Earth*, *125*, e2020JB019765. https://doi.org/10.1029/2020JB019765

Received 12 MAR 2020
Accepted 13 JUL 2020
Accepted article online 14 JUL 2020

Abstract The influence of confining and pore pressures on permeability and pore volume change was studied in two clayey sandstones. The coupling effect is characterized by the effective stress coefficients κ and β, respectively. Hydrostatic compression of a porous rock typically involves an initial nonlinear stage of elastic crack closure and a subsequent linear stage of pore deformation. To elucidate the influence of microcracks on the behavior, we measured the effective stress coefficients in these two stages separately. Our data show that the coefficients κ for permeability of both clayey sandstones are uniformly greater than 1, in agreement with published data and theoretical prediction for a microscopically inhomogeneous assemblage. Our data show that the presence of microcracks may homogenize the pore space, as reflected by a significantly lower κ value during the initial stage of nonlinear compression. We obtained some of the first measurements of the effective stress coefficient β for pore volume change in sandstones, which show values close to but uniformly less than 1. Synthesizing our sandstone data, recently published data on limestones, and theoretical analyses, we propose to define in the β-κ space two fundamentally different regimes for the effective stress behavior. A comparison of our data with Berryman's model, the clay shell model, and clay particle model indicates apparent discrepancies, which we propose to resolve with a dual equivalent-channel model based on the spatial partitioning of clayey and clay-free pore volumes.

1. Introduction

A physical understanding of the impact of tectonic stress and pore pressure on hydromechanical and fluid flow behaviors is critically important in many applications in rock physics, reservoir mechanics, seismotectonics, as well as geothermal and geotechnical engineering (Bredehoeft & Norton, 1990; Ingebritsen & Sanford, 2006; Mavko et al., 2009; Zoback, 2007). Experimental observations on porous rocks have demonstrated that the geophysical property of a saturated rock can often be characterized as a function of the effective stress $\sigma_{ij} - \xi P_P \delta_{ij}$, where σ_{ij} is the stress tensor (with compression taken as positive), P_P the pore pressure, and δ_{ij} the Kronecker delta. In this formulation the interplay of stress and pore pressure is encapsulated in the effective stress coefficient ξ.

Experimental data on the mechanical strength of rocks and soils show that it is typically changed by the mean stress and pore pressure in an equal and opposite manner, which would therefore imply an effective stress coefficient ξ equal to 1 (Baud et al., 2015; Jaeger et al., 2007; Paterson & Wong, 2005; Terzaghi, 1936). In contrast, measurement of other properties such as mechanical deformation (including bulk strain and pore volume change) and fluid transport has shown that the effective coefficients can be significantly different from unity. The magnitude of the coefficient and whether it is greater or less than 1 seem to depend on the geometry of the pore space and its mechanical responses, as well as the extent to which it can be idealized as microscopically homogeneous (Berryman, 1992; Nur & Byerlee, 1971; Walsh, 1981).

Extensive measurements have shown that values of the effective stress coefficient κ for permeability are less than or equal to 1 in crystalline rocks (Bernabe, 1986, 1987), jointed granite (Kranz et al., 1979), shale (Heller et al., 2014; Kwon et al., 2001), and the clay-free Fontainebleau sandstone (David & Darot, 1989). However, laboratory data for at least seven clayey sandstones have shown consistent values of $\kappa > 1$, ranging up to 7.1 (Al-Wardy & Zimmerman, 2004; Moghadam et al., 2016; Nur et al., 1980; Zoback, 1975; Zoback & Byerlee, 1975). First observed by Zoback and Byerlee (1975), who also proposed a heuristic model for this inequality, which predicts that the pore pressure is more effective than the confining pressure in changing the permeability, because of significant contrast between the clays and quartzo-feldspathic grains in their

mechanical responses. This "clay shell model" implicitly assumes that the clayey sandstone is microscopically inhomogeneous (Berryman, 1992). Wang et al. (2018) recently documented that the coefficient κ is uniformly larger than 1 in three limestones with dual porosity, which therefore indicates that they are analogous to clayey sandstones in being microscopically inhomogeneous.

The transport of fluid and development of pore pressure excess are controlled by the permeability and pore volume change, which hinge on the coupled effect of stress and pore pressure. Accordingly, it is important to simultaneously characterize the effective stress coefficients for permeability and pore volume change. However, as noted by Berryman (1992), for pore volume change there are basically no experimental data on its effective stress coefficient β. His theoretical analysis showed that if the rock can be idealized as microscopically homogeneous then the two coefficients obey the inequality $\beta \leq \kappa \leq 1$, but in the inhomogeneous case the value of β can be greater than or less than 1. Recently, Wang et al. (2018) conducted one of the first integrated measurements of both coefficients, and their data for three limestones with dual porosity show that values for not only κ but also β are greater than 1. Is their observation of such large values for both κ and β generally applicable to a microscopically heterogeneous rock, and in particular, the clayey sandstone? To systematically address this question, the first objective here is to simultaneously determine the coefficients κ and β in the clay-rich Berea and Boise sandstones.

Hydrostatic compression of a porous rock typically shows two stages: an initial nonlinear stage followed by a linear one, associated with elastic crack closure and pore deformation, respectively (Brace, 1965; Vajdova et al., 2004; Wong et al., 1997). The compressibility in the initial stage is significantly larger than the second, and given the contrast, it seems likely that the effective stress coefficients can attain quite different values. Since previous studies did not differentiate between the two different stages of deformation, our second objective is to clarify this question by probing the behaviors in the same sample for the two stages separately.

A number of micromechanical models have been developed to quantify the effective stress coefficient κ for permeability. Notable examples are the clay shell and clay particle models for clayey sandstone (Al-Wardy & Zimmerman, 2004), asperity contact model for fractures (Walsh, 1981), and pore shell model for oolitic limestone (Ghabezloo et al., 2009). A common feature of these models (with the exception of the clay particle model) is that their determination of κ is solely based on consideration of the pore volume change, with the premise that the coefficients κ and β for permeability and pore volume change are equivalent, which Berryman (1992) pointed out to be speculative. Indeed, his theoretical analysis suggested that the two coefficients can attain quite different values, and the data of Wang et al. (2018) for limestones and Meng et al. (2019) for deformed limestones show β values significantly lower than κ. Is this discrepancy between the two coefficients κ and β observed also in a clayey sandstone, and if so, how can existing models be modified to more realistically capture the laboratory data? Guided by our synthesis of the existing data on effective stress coefficients for permeability and deformation, our third objective is therefore to assess existing micromechanical models for discrepancy and develop an alternative model that would agree better with experimental observations.

2. Sample Materials and Experimental Procedure

The cylindrical samples of Berea and Boise sandstones were of nominal length 80 mm and diameter 40 mm, with parallel ends ground to ± 10 μm. X-ray powder diffraction (XRPD) was used to characterize the mineral composition, using the procedure as described by Heap et al. (2017). The XRPD analyses were performed on powder mounts using a PW 1800 X-ray diffractometer and the phases in the whole rock powders were quantified using the Rietveld program BGMN (Bergmann et al., 1998). In terms of weight percentage, Berea sandstone has 89.2% quartz, 2.1% K-feldspar, 1.9% albite, and 6.3% clays (including 3.8% illite/muscovite, 2% kaolinite, and 0.5% chlorite-smectite); and Boise sandstone has 45.8% quartz, 8.9% K-feldspar, 23% albite, 12.7% clays (including 10.3% illite/muscovite and 2.4% dioctahedral smectite), and 2.1% clinoptilolite. With very little to faint laminations, the two sandstones are considered to be isotropic, as reflected by relatively small difference between *P* wave velocities in different directions. Under ambient conditions of pressure and temperature, the velocities along and transverse to the cylindrical axis are 2.23 and 2.33 km/s in a Berea sandstone sample, and 3.02 and 2.90 km/s in a Boise sandstone sample. Based on the mineral content and dry weight of sample, the average porosities for our Berea and Boise sandstone samples can be

Table 1
Basic Physical Information and Experimental Description of the Tested Clayey Sandstones

Rock	Number	Porosity	Condition	Comment
Berea	Be01	0.208	Hydrostatic loading, Pp = 1 MPa	Hydrostatic loading from 5 to 90 MPa at the nominal rate of 1 MPa/min
	Be02	0.203	Hydrostatic loading for studying effective stress behavior	Permeability and pore volume change were measured under increasing confining pressure for three different pore pressures
Boise	Bo01	0.303	Hydrostatic loading, Pp = 1 MPa	Hydrostatic loading from 5 to 85 MPa at the nominal rate of 1 MPa/min
	Bo02	0.299	Hydrostatic loading for studying effective stress behavior	Permeability and pore volume change were measured under increasing confining pressure for three different pore pressures

calculated with value of 20.5% and 30.0% referring to a solid grain density of 2,644.6 kg/m^3 for Berea and 2,652.2 kg/m^3 for Boise, respectively (Table 1).

Hydromechanical measurements at room temperature were performed using a triaxial test rig acquired from Sanchez Technology, detailed description of which was presented by Wang et al. (2018). The confining medium was silicone oil, and pressure up to 100 MPa can be generated by a servo-controlled volumetric pump. The pressure was monitored by a transducer with an accuracy of 0.01 MPa. Samples were jacketed with a neoprene sleeve. Before each measurement a sample was first evacuated, and then injected with the pore fluid (deionized water). A protocol analogous to that of Wang et al. (2018) was adopted to ensure that the fluid-rock system had attained equilibrium before the initiation of a hydromechanical experiment on the saturated sample. To measure the poroelastic behavior and effective stress coefficients, the sample must sustain a relatively stable microstructure, so that the pore volume and permeability changes remain basically reversible with minimal hysteresis during cyclic loading in confining and pore pressures. This was achieved by subjecting a sample to several cycles of seasoning, following a protocol similar to that of Wang et al. (2018).

If the pore pressure upstream is different from that downstream, the fluid would flow in an axial direction. To evaluate the permeability on the basis of Darcy's law, the differential pore pressure that was required to maintain a steady flow rate of 0.1 ml/min was determined. As for the pore volume change, measurements were made between sequential stress states, with either a change in confining pressure while keeping the pore pressure constant, or a change in pore pressure while keeping the confining pressure constant. For the former stress state, the pore volume change was inferred directly from relative positions of the syringe pumps. For the latter, the pore volume change is more challenging to measure and difficult to resolve, because one has to deduct the volume change associated with compressibility of the saturating fluid and

Table 2
Description of Samples Whose Effective Stress Coefficients are Plotted in Figures 12 and 13

Porosity range	Rock type	Clay fraction	Porosity	κ	β	Source
$\phi \leq 0.1$	Knorringfjellet	0.006	0.09	1.4	-	Moghadam et al. (2016)
					-	
$0.1 < \phi \leq 0.2$	St. Peter	0.005	0.20	1.2	-	Nur et al. (1980)
	Stainton	0.08	0.16	5.4	-	Al-Wardy and Zimmerman (2004)
	Berea (|| bedding)	0.08	0.19	2.2	-	Zoback and Byerlee (1975)
	Berea (⊥ bedding)	0.08	0.19	4.0	-	Zoback and Byerlee (1975)
	Berea 100	0.086	0.20	3.3	-	Nur et al. (1980)
	Berea at Stage I	0.1[a]	0.20	1.5	1	This study
	Berea at Stage II	0.1[a]	0.20	4.1	0.85	This study
	Bandera	0.20	0.16	7.1	-	Nur et al. (1980)
$\phi > 0.2$	Berea 500	0.043	0.21	4.6	-	Nur et al. (1980)
	Berea 500(brine)	0.043	0.21	3.2	-	Nur et al. (1980)
	Brownstone	0.045	0.21	2.4	-	Nur et al. (1980)
	Berea	0.048	0.22	2.6	-	Moghadam et al. (2016)
	Massillon	0.05	0.23	3.2	-	Nur et al. (1980)
	Massillon	0.06	0.24	3.5	-	Zoback (1975)
	Berea 350	0.06	0.22	2.2	-	Nur et al. (1980)
	Berea 350(brine)	0.06	0.22	2.9	-	Nur et al. (1980)
	Berea 200	0.063	0.22	3.2	-	Nur et al. (1980)
	Boise	0.13[a]	0.30	1.3	1	This study

[a]Data reference from Wong et al. (1997).

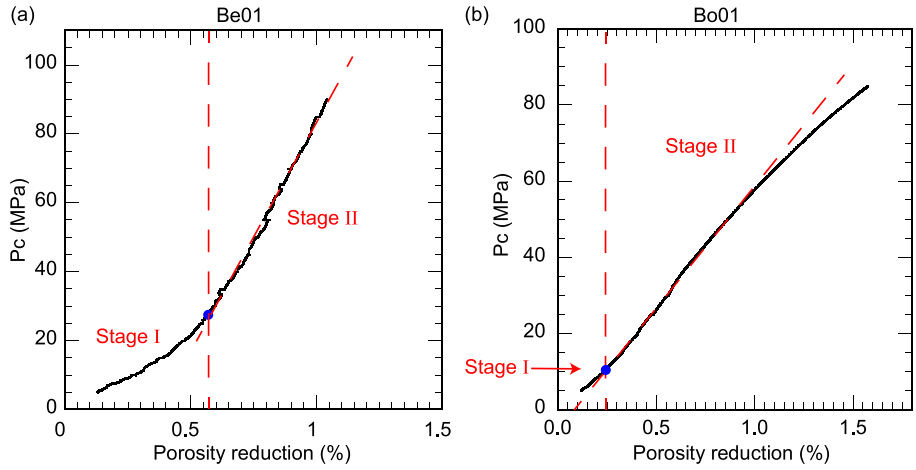

Figure 1. Mechanical data for water-saturated Berea and Boise sandstones at constant pore pressure of 1 MPa under hydrostatic loading. (a) Confining pressure as a function of porosity reduction for Be01 ranging from 5 to 90 MPa, (b) confining pressure as a function of porosity reduction for Bo01 ranging from 5 to 85 MPa. Hydrostatic compression involves an initial nonlinear stage I of elastic crack closure and a subsequent linear stage II of pore deformation. The critical pressure for crack closure is 27 MPa for Be01 and 10 MPa for Bo01, respectively. Based on the linear relation, the corresponding inferred crack porosity is 0.38% for Be01 and 0.08% for Bo01.

storage capacity of the pore pressure system (Fatt, 1958). Our calibration and data reduction procedures were analogous to that described by Wang et al. (2018) in their Appendix A.

3. Hydromechanical Data

In presenting our mechanical data, we have adopted the convention that compressive stresses and strains are considered positive. Experimental conditions of the mechanical tests are compiled in Table 1.

3.1. Two Stages of Hydrostatic Compression

To differentiate between the two stages of hydrostatic compression associated with elastic crack closure and pore deformation, two samples (Berea sandstone Be01 and Boise sandstone Bo01) were conducted at constant pore pressure $P_p = 1$ MPa over broad ranges of confining pressure (P_c = 5–85 MPa for Be01 and 5–90 MPa for Bo01). Confining pressure was increased at a nominal rate of 1 MPa/min, considered to be slow enough to ensure drained deformation induced by the compression. Porosity reduction as a function of confining pressure for Be01 and Bo01 are shown in Figures 1a and 1b, respectively. It typically shows a transition of the hydrostatic compression behavior from an initial nonlinear stage to a linear stage, which we will

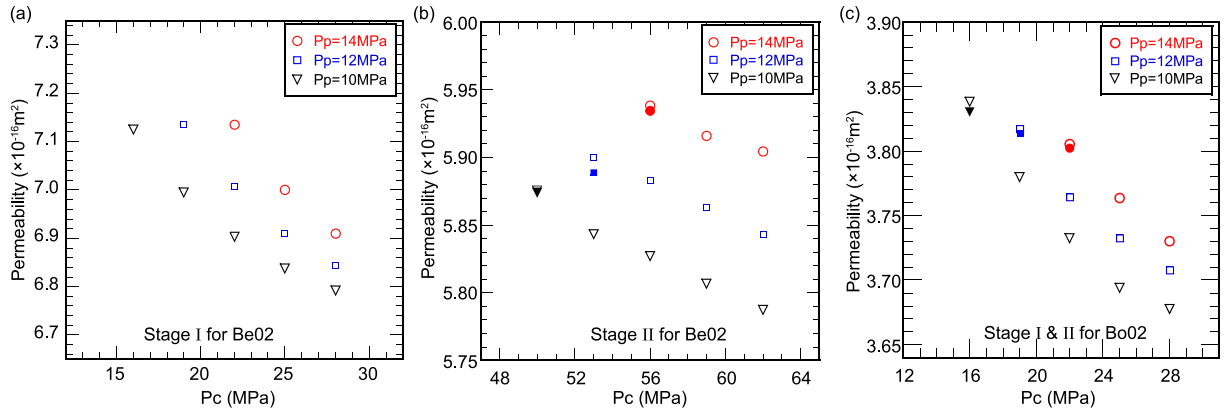

Figure 2. Permeability as a function of confining pressure for three different pore pressures for Berea and Boise sandstones marked using the open symbols for loading and solid symbols for unloading. (a) Stage I for Be02, (b) stage II for Be02, (c) stages I and II for Bo02.

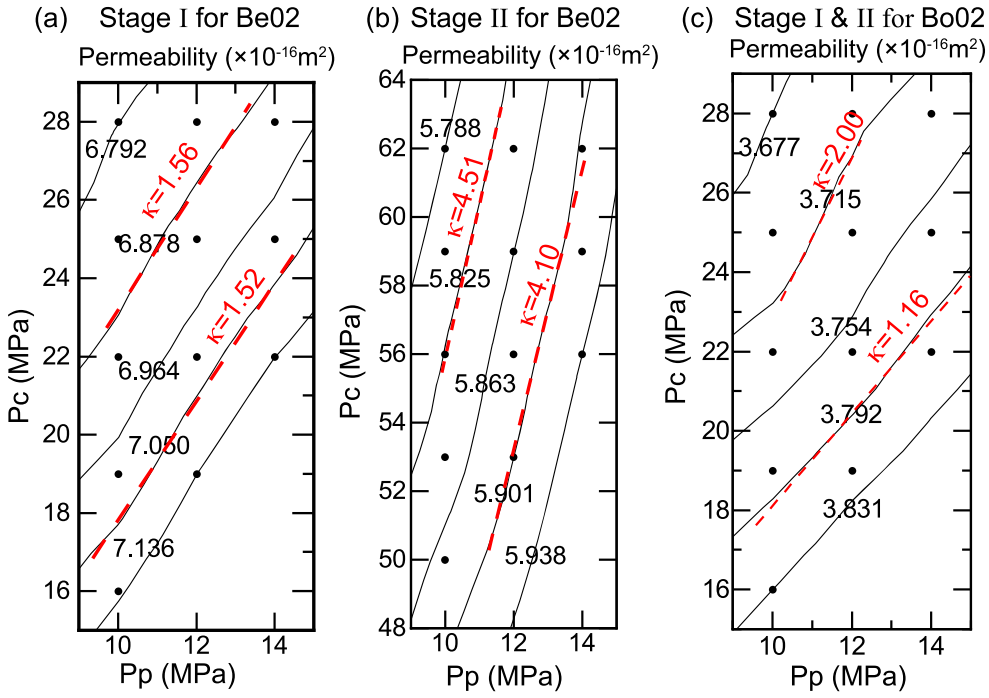

Figure 3. Iso-permeability contours presented in a confining pressure and pore pressure space for Berea and Boise sandstones. (a) Stage I for Be02, (b) stage II for Be02, (c) stages I and II for Bo02. The corresponding effective stress coefficients for permeability κ, calculated by linear interpolations (red dashed lines), are also given.

refer to as "stage I" and "stage II," respectively. Such a transition has been observed in various rocks, including granite (Brace, 1965), limestone (Vajdova et al., 2004), and sandstone (Wong et al., 1997). Walsh (1965) showed that the nonlinearity in stage I and the linear behavior of stage II can be attributed to elastic crack closure and deformation of relatively equant pores, respectively. He further proposed that one can extrapolate the linear behavior in stage II and infer the crack porosity as the intercept at the horizontal axis.

Using Walsh's (1965) approach, the crack porosities of our Berea and Boise sandstones samples were inferred to be 0.38% and 0.08%, respectively. From our data, we can identify the transition from stage I to II at Terzaghi effective pressures (P_c-P_p) of around 27 MPa for Berea sandstone (Figure 1a) and 10 MPa for Boise sandstone (Figure 1b), respectively. Because the transition pressure was relatively high in Berea sandstone, it was feasible to characterize the effective stress behavior separately in stages I and II. As for Boise sandstone, such a separation was not practical and our measurement extended over both stages.

3.2. Permeability as a Function of Confining and Pore Pressures

Two sets of experiments were conducted on Berea sandstone sample Be02, first in stage I and then in stage II. One set of experiment was conducted on Boise sandstone sample Bo02, at conditions that span over both stages. Each of the three sets includes three cycles of increasing and decreasing confining pressures at fixed pore pressures of 14, 12, and 10 MPa. For example, the stage I measurement for Be02 (Figure 2a) began with the first cycle at pore pressure of 14 MPa and confining pressure of 22 MPa, which was then increased in two steps to 28 MPa. The confining pressure was then decreased in one step to the initial value of 22 MPa, after which the confining and pore pressures were adjusted to initiate the second cycle at pore pressure of 12 MPa. In the two sets of experiment in stage II of Be02 (Figure 2b) and stages I and II of Bo02 (Figure 2c), we also acquired data (solid symbols) at the end of each cycle at a fixed pore pressure. It can be seen that in spite of the seasoning a small amount of hysteresis would develop, indicating a slight decrease in permeability after a confining pressure cycle.

The evolution of permeability was qualitatively similar in all three sets of data. At a fixed pore pressure, a nonlinear decrease of permeability with increasing confining pressure was observed, except for stage II of Be02 that seems almost linear, possibly because it derives primarily from pore deformation. In general,

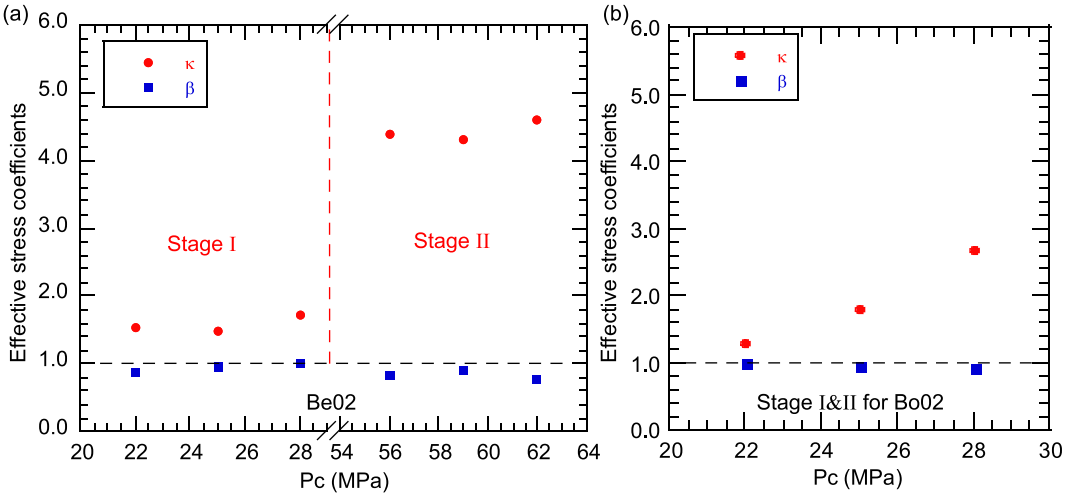

Figure 4. Effective stress coefficients κ and β as a function of confining pressure for (a) Berea and (b) Boise sandstones.

the change of permeability in response to a perturbation in pore pressure was greater than the corresponding response to confining pressure. This predominate influence of pore pressure on permeability is particularly significant in stage II of the Berea sandstone sample (Figure 2b).

By interpolation of our experimental data, iso-permeability contours were constructed in the P_c-P_p space. Most of the contours were observed to follow an approximately linear trend, with slopes that correspond to the effective stress coefficients κ. For Berea sandstone there is a significant increase in its κ value from stage I (Figure 3a) to stage II (Figure 3b). Previous studies of the same sandstone have reported values of 2.2, 4.0 (Zoback & Byerlee, 1975), and 3.3 (Walls & Nur, 1979), which are comparable to our data for stage II subsequent to elastic crack closure. Although κ values of Boise sandstone (Figure 3c) are lower than Berea sandstone, they are greater than 1 and thus consistent with published data for other clayey sandstones.

In all three sets of data in Figure 3, one can observe an overall trend for the inferred κ value to increase somewhat with increasing confining pressure and decreasing pore pressure. To characterize the effect of confinement on the coefficient κ, we note that an incremental change of the permeability k derives from two contributions associated with incremental changes in confining pressure P_C and pore pressure P_P, respectively:

$$\delta k=\frac{\partial k}{\partial P_C}\delta P_C+\frac{\partial k}{\partial P_P}\delta P_P=\frac{\partial k}{\partial P_C}(\delta P_C-\kappa\delta P_P), \tag{1a}$$

and accordingly the effective stress coefficient κ for permeability can be evaluated as

$$\kappa=-\left(\frac{\partial k}{\partial P_P}\right)/\left(\frac{\partial k}{\partial P_C}\right). \tag{1b}$$

For the three sets of data presented in Figures 2a and 2c, we estimated the denominator in 1b by first fitting the data at the intermediate pore pressure with a quadratic relation (between k and P_c), and then differentiating it to estimate the derivative $\frac{\partial k}{\partial P_C}$ as a function of P_c. For the data in Figure 2b, a linear relation was used and the derivative estimated from the average slope. At a given confining pressure, we can also estimate the numerator $\frac{\partial k}{\partial P_P}$ as the ratio of two terms: the permeability measured at the maximum pore pressure minus that at the minimum, and the maximum pore pressure minus the minimum. The denominator and numerator so evaluated were then input into 1b to determine the coefficient κ for a given confining pressure. For Berea sandstone, the effective stress coefficient κ shows significant increase from stage I to stage II (Figure 4a), and within each stage it also increases somewhat with confinement. For Boise sandstone, the

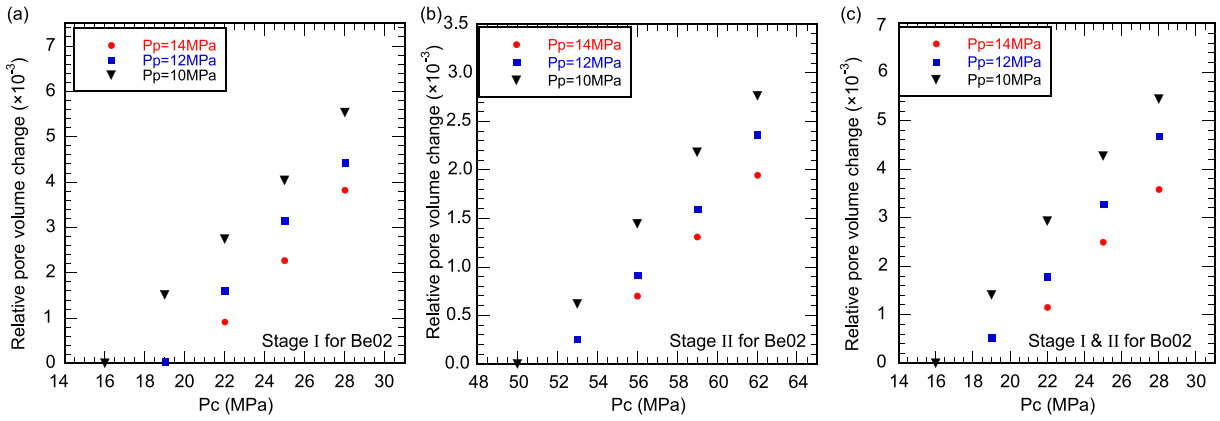

Figure 5. Relative pore volume change as a function of confining pressure for three different pore pressures of Berea and Boise sandstones: (a) stage I for Be02, (b) stage II for Be02, (c) stages I and II for Bo02.

increase of κ with confinement seems more pronounced (Figure 4b), possibly due to the transition from stage I to II embedded in the data set.

3.3. Pore Volume Change as a Function of Confining and Pore Pressures

Relative pore volume change e_ϕ is defined to be the pore volume change δV_v normalized by the initial pore volume V_v. Our data presented in Figures 5a and 5b (stages I and II of Be02) and Figure 5c (Bo02) show that e_ϕ decreased with increasing confining pressure and decreasing pore pressure in an approximately linear manner. Magnitude of the relative change was on the order of 10^{-3}, and in contrast to the predominate influence of pore pressure on permeability shown in Figure 2, the effects of pore pressure and confining pressure on pore volume change were comparable.

We plot in the P_c-P_p space contours of equal e_ϕ as constrained by our data. Most of the contours follow an approximately linear trend, with slopes which correspond to the effective stress coefficients β. For Berea

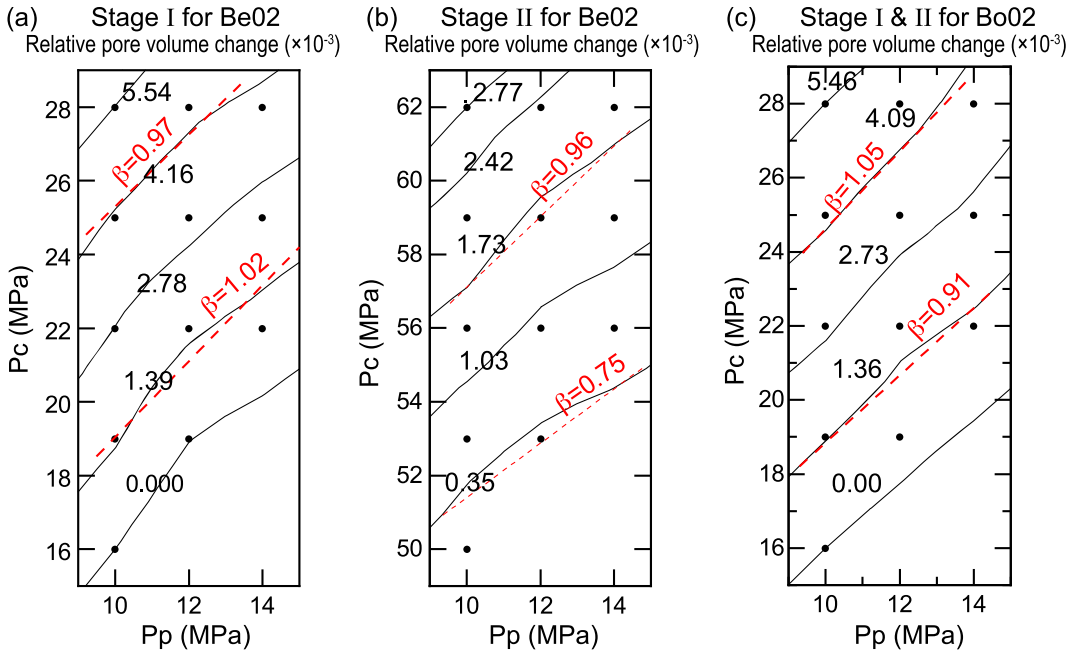

Figure 6. Iso-pore volume change contours presented in a confining pressure-pore pressure space for Berea and Boise sandstones. (a) Stage I for Be02, (b) stage II for Be02, (c) stages I and II for Bo02. The corresponding effective stress coefficients for pore volume change β, calculated by linear interpolations (red dashed lines), are also given.

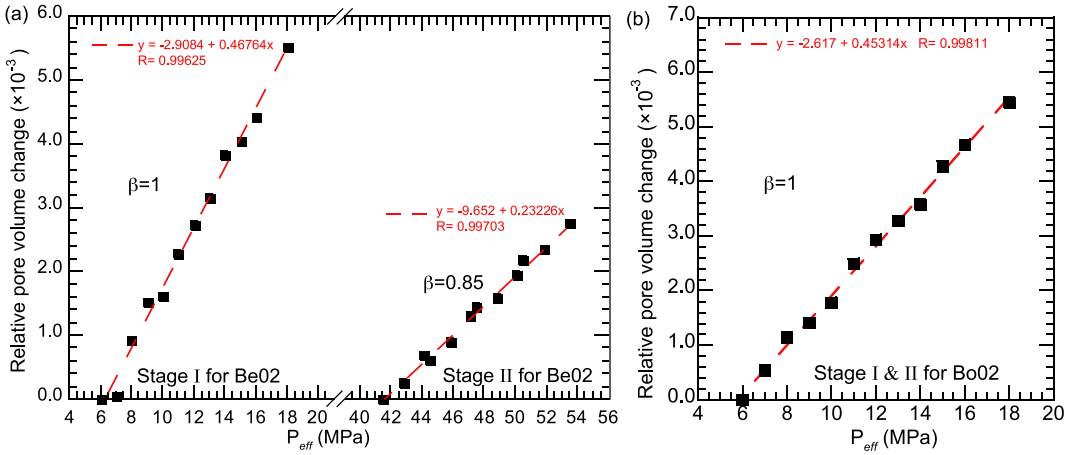

Figure 7. Relative pore volume change as a function of effective stress for (a) Berea (Be02) and (b) Boise (Bo02) sandstones. The effective stress was calculated using values of the effective stress coefficients for pore volume change β indicated on the graphs. The measurements are shown as black squares. The red lines correspond to linear fits based on the equations shown on the graphs.

sandstone, measured values of β were close to 1 in stage I (Figure 6a) and somewhat lower in stage II (Figure 6b). For Boise sandstone (Figure 6c), the values were all close to 1.

To characterize the effect of confinement on the coefficient β, we again note that an incremental change of the relative pore volume change e_ϕ derives from two contributions associated with incremental changes in confining pressure P_C and pore pressure P_P, respectively:

$$\delta e_\phi = \frac{\partial e_\phi}{\partial P_C}\delta P_C + \frac{\partial e_\phi}{\partial P_P}\delta P_P = \frac{\partial e_\phi}{\partial P_C}(\delta P_C - \kappa \delta P_P), \tag{2a}$$

and accordingly the effective stress coefficient β for pore volume change can be evaluated as

$$\beta = -\left(\frac{\partial e_\phi}{\partial P_P}\right) / \left(\frac{\partial e_\phi}{\partial P_C}\right). \tag{2b}$$

For the three sets of data presented in Figure 5, we estimated the denominator in 2b by fitting the data with a linear relation (between e_ϕ and P_c) and then evaluated the derivative $\frac{\partial e_\phi}{\partial P_C}$ as constant equal to the slope. The numerator $\frac{\partial e_\phi}{\partial P_P}$ was evaluated as the ratio of two terms: value of e_ϕ measured at the maximum pore pressure minus that at the minimum, and the maximum pore pressure minus the minimum. The effective stress coefficients β so evaluated for all three sets of data have two common features. First, they all show minimal dependence on confinement, with values close to 1 in stage I (Figure 4a) of Berea sandstone and stages I and II (Figure 4c) of Boise sandstone, and somewhat lower values in stage II of Berea sandstone (Figure 4b). Second, under identical confinement the effective stress coefficient β for pore volume change is consistently smaller than the corresponding coefficient κ for permeability.

Given that the inferred values of β are almost constant in each of the three sets of data, it seems reasonable to adopt a constant β value for evaluating the effective pressure. Data for three cycles at three different pore pressures can then be collapsed into one curve with e_ϕ plotted versus effective pressure $P_C - \beta P_P$, with constant values of $\beta = 1$ and 0.85 for stages I and II of Berea sandstone (Figure 7a), and 1 for Boise sandstone (Figure 7b). From linear regression of the three sets data, we determined the correlation coefficients to be 0.99 with slopes (which correspond to the pore compressibilities) of $\beta_\phi = 0.47$/GPa and 0.23/GPa, in stages I and II of Be02, and $\beta_\phi = 0.45$/GPa, in stages I and II of Bo02, respectively. These are comparable to sandstone values compiled by David et al. (1994), and as expected the compressibility of Berea sandstone in stage II was relatively low since it was dominated by pore deformation.

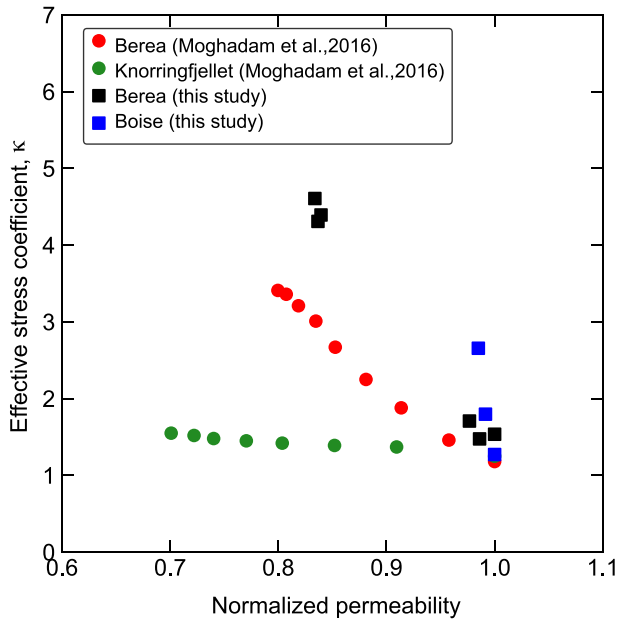

Figure 8. Effective stress coefficient κ for permeability as a function of normalized permeability referring to higher permeability with value of 9.576×10^{-14} m^2 for Berea in Moghadam et al. (2016), 3.3×10^{-17} m^2 for Knorringfjellet in Moghadam et al. (2016), 7.01×10^{-16} m^2 for Berea in this study, and 3.76×10^{-16} m^2 for Boise in this study.

4. Discussion

4.1. Effective Stress Coefficients for Permeability and Pore Volume Change

We conducted a systematic investigation of the effective stress behaviors for permeability and pore volume change in two relatively isotropic clayey sandstones over a broad range of hydrostatic pressure condition. To our knowledge, there have not been any such studies of the coefficient β for pore volume change in sandstones, and our new data thus fill in a critical gap. In contrast, there have been numerous studies of the coefficient κ for permeability in clayey sandstones (Al-Wardy & Zimmerman, 2004; Moghadam et al., 2016; Nur et al., 1980; Zoback & Byerlee, 1975), with a primary focus on the control of clay content over the value of κ. However, given that the permeability evolution is sensitively dependent on the closure and opening of microcracks by the confining and pore pressures, it seems likely that the presence of microcracks can also influence the effective stress behavior, but this aspect has not been investigated systematically. Because hydrostatic compression of a porous rock typically involves an initial nonlinear stage I of elastic crack closure and a subsequent linear stage II of pore deformation, in this study we differentiated between the two different stages in Berea sandstone and characterized the effective stress coefficients κ and β in these two stages separately.

For Berea sandstones, Zoback and Byerlee (1975) reported values of 2.2 and 4.0 for its effective stress coefficient for permeability, and latter measurements (Nur et al., 1980) show higher values up to 7.1. While the variability can partly be attributed to differences in mineralogy and porosity, our study also underscores the significant influence of microcracks and their closure on the effective stress behavior. In the transition from stage I to II, the closure of ~0.38% crack porosity in Be02 (Figure 1) increased the value of κ by a factor of >2 (Figure 4a). This implies that the lower values of κ in stage I are related to the presence of randomly distributed microcracks that would alleviate the microscopic inhomogeneity. It should also be noted that Zoback and Byerlee (1975) suggested that, because their two samples were cored parallel and perpendicular to bedding, bedding anisotropy may also be an important factor. However, given the relatively isotropic nature of Berea sandstone, bedding seems unlikely to be a dominant factor on the effective stress behavior, but this issue warrants further investigation in the future.

For Boise sandstone, the effective stress coefficient κ has values greater than 1 similar to other clayey sandstones. We were not able to conduct measurements separately in two stages, but our data indicate an increase of the coefficient κ with increasing confinement and crack closure, also by a factor of >2 (Figure 4b). Because the closure of microcracks is accompanied by permeability reduction, one would therefore expect the coefficient κ to increase with decreasing permeability k. Our data for κ as a function of k of Berea and Boise sandstones are plotted in Figure 8, and for comparison we also include the recent data of Moghadam et al. (2016) for Berea and Knorringfjellet sandstones. The latter sandstone has a relatively low porosity of 9% and permeability on the order of 10^{-17} m^2. Notwithstanding the difference in permeability, the data indeed all follow a similar trend, in that the effective stress coefficient κ for permeability would increase with decreasing permeability k.

Our data for pore volume change (Figure 4) show that both clayey sandstones have β values close to unity (ranging from 0.88 to 1.05), except for Berea sandstone in stage II with lower values (ranging from 0.79 to 0.93). We are not aware of any other published data for comparison. However, there have been theoretical predictions by Berryman (1992) who derived a relation connecting β, χ (effective stress coefficient for porosity change), and α (Biot's effective stress coefficient for bulk strain) and ϕ (porosity):

$$\alpha \leq \beta = \chi - \phi(\chi/\alpha - 1) \leq \chi. \tag{3a}$$

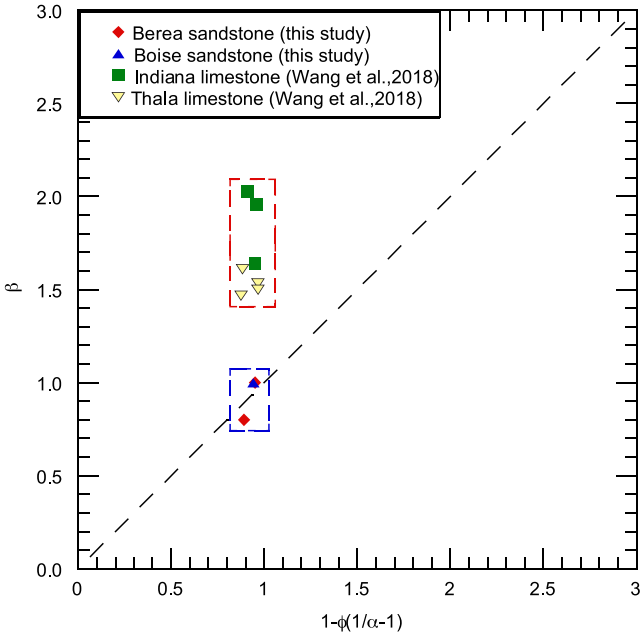

Figure 9. Measured values of the effective pressure coefficient β for pore volume change for Berea and Boise sandstones (this study), and Indiana and Thala limestones (Wang et al., 2018) as a function of the theoretical prediction (Equation 3b) for a microscopically homogeneous rock.

The above relation is generally applicable independent of whether the rock is microscopically homogeneous or heterogeneous. Furthermore, for a microscopically homogeneous rock, Berryman (1992) showed that the value of χ should be exactly 1, and we expect then

$$\beta=1-\phi(1/\alpha-1). \tag{3b}$$

First derived by Zimmerman et al. (1986), Equation 3b provides a criterion to assess whether a rock can be idealized as microscopically homogeneous, and any disparity between experimental data and the criterion can accordingly be attributed to microscopic inhomogeneity in the rock. Although we did not experimentally measure Biot's coefficient α, it can be inferred from our compressibility measurements (Figure 7) as explained in Appendix A. We compare our experimental data with the value of β expected of a microscopically homogeneous rock according to 3b. As illustrated in Figure 9, whereas our data for Berea sandstone in stage II fall below the predicted values for a microscopically homogeneous rock, the rest of them fall above. For comparison, we also plot the data of Wang et al. (2018) for three limestones with dual porosity, which have values of β uniformly larger than 1 that deviate significantly from the prediction for a microscopically homogeneous rock.

4.2. Two Regimes of Effective Stress Behavior

The availability of relatively complete data on both effective stress coefficients for permeability and pore volume change has motivated up to map out the coefficients (κ, β) and identify two fundamentally different regimes of effective stress behavior. Regime I corresponds to a microscopically homogeneous rock, for which Berryman (1992) concluded that its effective stress coefficients and porosity obey the following relation:

$$\phi \le \alpha \le \beta \le \kappa \le \chi=1. \tag{4}$$

On a κ-β map, the effective stress coefficients of such a rock should accordingly fall in the triangular region marked as Regime I in Figure 10.

Any rock with $\kappa > 1$ is microscopically inhomogeneous and would fall in the rectangular region marked as Regime II. The two clayey sandstones investigated in this study and three limestones with dual porosity (Wang et al., 2018) have comparable κ values and belong to this regime. However, because their β values are significantly different (Figure 10), it suggests further breaking down this regime into Regimes IIA and IIB, according to whether the effective stress coefficient for pore volume change is less than or greater than 1, respectively.

It should be noted that, since this classification of the effective stress behavior is based on available data for only five sandstones and limestones, it is by no means definitive and may need to be refined when more comprehensive data for different rock types are available from future studies. Extensive measurements on crystalline rocks (Bernabe, 1986, 1987; Coyner, 1984), shale (Heller et al., 2014; Kwon et al., 2001), and a limestone dominated by macroporosity (Wang et al., 2018) have shown κ values less than unity, which would suggest that these rocks can be approximated as microscopically homogeneous. However, we cannot confirm that indeed they belong to Regime I until we have available systematic measurements of the coefficient β for these rock types. Also, it should be emphasized that the classification scheme here is based solely on the two effective stress coefficients κ and β of a porous rock, which should not be construed as a direct measure of the degree of heterogeneity of its microstructure. Indeed, there remain many fundamental questions on how the effective stress behavior is related to the microstructure, which are highlighted in the following discussion on the various modeling schemes.

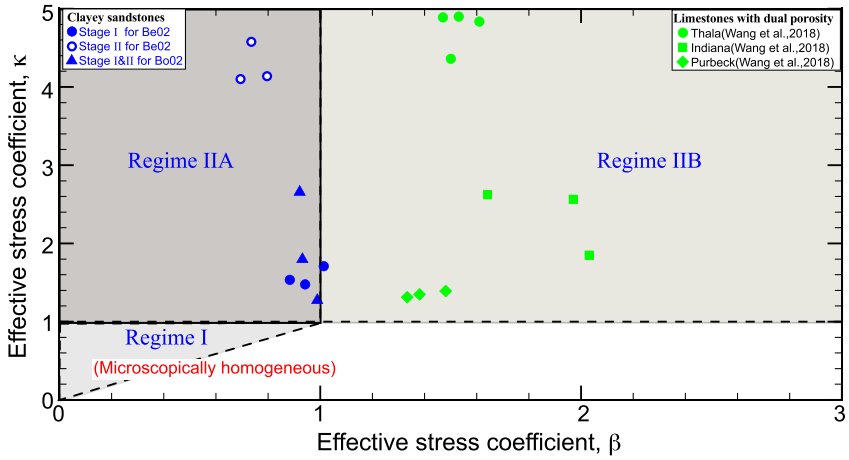

Figure 10. Regimes for effective stress behavior of porous rocks. Regime I is for microscopically homogeneous rocks, with value $\beta \leq \kappa \leq 1$, Regime II is for inhomogeneous rocks with value $\kappa > 1$, where Regime IIA is for clayey sandstones, with value $\beta \leq 1$, and Regime IIB is for limestones with dual porosity, with value $\beta > 1$.

4.3. Comparison With Berryman's Clayey Sandstone Model

With a clayey sandstone in mind, Berryman (1992) formulated a model for a microscopically inhomogeneous aggregate with two distinct constituents. As illustrated in Figure 11, the constituent 1 (presumably embedded with clays and microcracks) is interconnected, percolative, and expected to have a very soft frame modulus $K^{(1)}$. In contrast, the constituent 2 is considered to be made up of solid grains that are isolated and relatively impermeable (Figure 11). For this model configuration, Berryman (1992) derived a relation among the effective stress coefficients of such a clayey sandstone, which can now be tested with the comprehensive data now available. The effective stress coefficient κ for permeability is predicted to be related to the coefficients α for strain and χ for porosity change according to

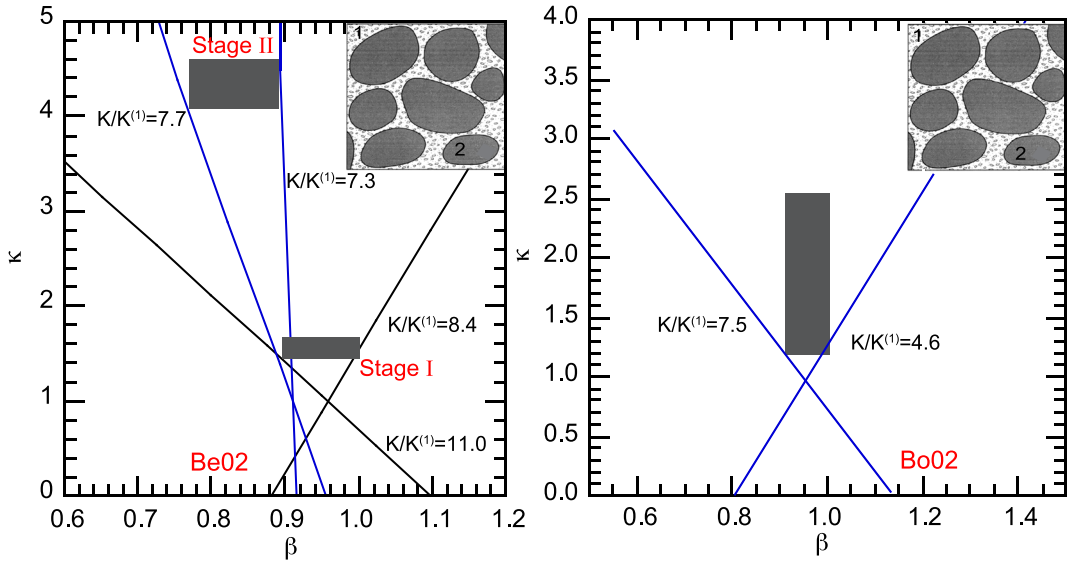

Figure 11. Effective stress coefficient κ for permeability as a function of effective stress coefficient for pore volume change β. (a) The gray box indicates the data ranges for Berea sample in stage I and stage II. These data can be bracketed by the theoretical predictions of Berryman's model for values of $K/K^{(1)}$ between 8.4–11.0 in stage I and 7.3–7.7 in stage II. (b) Data on Boise sandstone could also bracketed by the ratio $K/K^{(1)}$ between 4.6 and 7.5.

$$\kappa = \alpha + \frac{3n_1(\alpha-\phi)(\chi-\alpha) - 3q\phi(\theta-\alpha)\frac{K}{K^{(1)}}}{3n_1(\alpha-\phi) + 2\phi - 3q\phi\frac{K}{K^{(1)}}}. \quad (5)$$

Because relation 3a is generally applicable to porous rocks, it can be used to connect the effective stress coefficient β for pore volume change with the porosity ϕ, as well as coefficients χ and α. The parameter θ is the ratio of the macroscopic increments of confining and pore pressures such that the relative change in volume of each constituent is the same (Berryman & Milton, 1991), and according to Berryman (1992), relevant laboratory data have indicated $\theta \approx 1$. Although the pore geometry was not specified in the model, it was necessary to assume that the transport properties and porosity are related by power laws: the exponent n_1 in 5 is associated with the power law for the permeability of constituent 1, and the cementation exponent m_1 is for Archie's law. In our calculations here, we followed Berryman (1992) to assume $n_1 = 4$, $m_1 = 2$ and the remaining parameter $q \approx n_1\text{-}m_1\text{–}2/3 = 1.333$.

Using the α values inferred in Appendix A, Equations 5 and 3a can then be used to predict the coefficient κ of clayey sandstone as a function of the coefficient β for a given modulus ratio $K/K^{(1)}$. For the parameter ranges of interest here, Berryman's (1992) model predicts that κ and β fall on approximately linear trends. Our data for Berea sandstone can be bracketed by lines corresponding to $K/K^{(1)} = 8.4$–11.0 in stage I, and 7.3–7.7 in stage II (Figure 11a). The Boise sandstone data can also be bracketed by the lines corresponding to $K/K^{(1)} = 4.6$ and 7.5 (Figure 11b). These values of bulk modulus ratio are comparable to the value of 10 suggested by Berryman (1992) and what has been inferred from the clay shell model to be discussed next. With crack closure the bulk moduli are expected to both increase in stage II, but the enhancement is expected to be proportionately weaker in the bulk rock than in constituent 1 where the microcracks are embedded, and accordingly the ratio $K/K^{(1)}$ is likely to decrease with the transition from stage I to II.

Berryman's (1992) model for clayey sandstone has provided useful insights into how microscopic inhomogeneity in the form of mechanical contrast between the isolated solid grains and the soft percolative matrix can influence the relative magnitudes of the effective stress coefficients for permeability, pore volume change, and strain. Although the model is quite general without any specific assumptions regarding the geometry of the grains or pore space, this approach has an intrinsic limitation in that it does not address the micromechanical basis of the effective stress behavior.

4.4. The Clay Shell and Clay Particle Models

One model that attempts to capture how grain-scale deformation and fluid flow control the effective stress coefficient for permeability is the clay shell model (Al-Wardy & Zimmerman, 2004; Zoback & Byerlee, 1975). The conduit for flow in a clayey sandstone is idealized as an equivalent channel lined with a clay shell. Cylindrical in geometry, the channel has a cross-section with an inner void (of radius a) enclosed in a shell of clays (with radius between a and c), which is in turn embedded in a concentric shell of quartzo-feldspathic grains (of external radius b) (Figure 12). Because the clay shell is more compliant than the outer grain layer, an increase of pore pressure is more effective than a corresponding decrease in confining pressure in dilating the inner void and enhancing the permeability. In this idealized model, the permeability k depends solely on the radius a, which implies that the effective coefficient defined in 1b can be written as $= -\left(\frac{\partial a}{\partial P_P}\right)/\left(\frac{\partial a}{\partial P_C}\right)$

Al-Wardy and Zimmerman (2004) presented a comprehensive analysis of the clay shell model, their results of relevance to the present study are summarized in Appendix B. The model predicts that the effective stress coefficient κ is related to the ratio γ between the shear moduli of the external grain layer and the clay shell, porosity ϕ, and volumetric clay fraction f_c according to

$$\kappa = \frac{[f_c(1-\phi)+\phi+2][2f_c(1-\phi)+3\phi] + 2\gamma f_c(1-f_c)(1-\phi)^2}{9[f_c(1-\phi)+\phi]}. \quad (6)$$

For mathematical convenience, we here follow Al-Wardy and Zimmerman (2004) to assume that the two concentric layers have identical Poisson's ratio of 0.25. They considered a single porosity (20%), and here

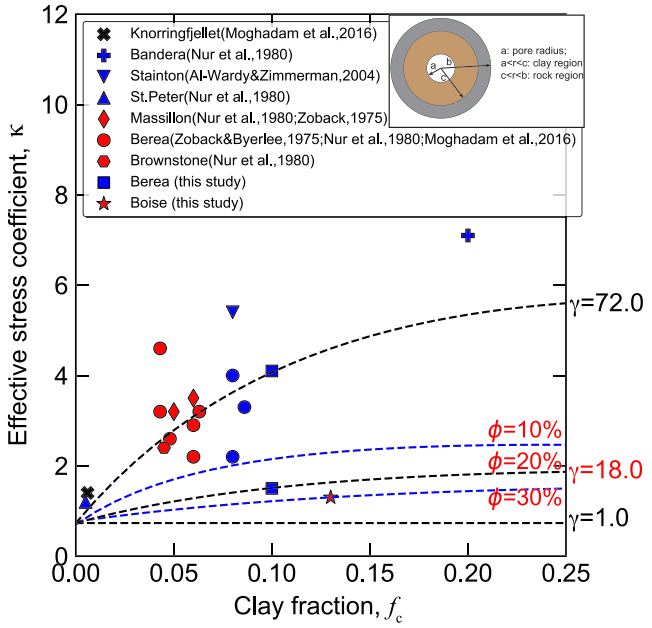

Figure 12. Effective stress coefficient as a function of clay fraction for different porosities and shear modulus ratio using the clay shell model. The points are data from this study and from the literature (see Table 2), and the black line refers to clay shell model using the different ratio between rock and clay stiffness at the fixed porosity of 20%, blue dashed lines refer to clay-particle model using the different porosities of 10%, 20%, and 30% at the constant shear ratio of 18.0 with the Poisson ratio of rock and clay taken as 0.25.

we have extended to two other porosities (10% and 30%). The model predicts that the coefficient κ increases with increasing clay fraction and modulus contrast, and it also decreases somewhat with increasing porosity (Figure 12).

For comparison with the model prediction, we have compiled laboratory data for the effective stress coefficient κ of eight clayey sandstones (Knorringfjellet, St. Peter, Stainton, Berea, Bandera, Brownstone, Massillon, and Boise sandstone) with clay content ranging from 0.5% to 20% and porosity from 9% to 30%. In previous studies, the clay contents were in terms of volume or weight, and in some case not specified. We have lumped them together here, with the assumption that the difference is likely small. In qualitative agreement with the model, there is an overall trend in the laboratory data for porosity in the range of 11–20% (blue symbols in Figure 12) for the κ value to increase with increasing clay content. However, data for porosity >20% (red symbols) apparently follow an opposite trend, with our Boise sandstone sample showing a relatively low κ value even though it has the highest clay content in the group. To bracket all the experimental data, one must resort to a shear modulus ratio γ as large as 72 (Figure 12). Al-Wardy and Zimmerman (2004) pointed out that such a high ratio seemed unrealistic, and accordingly they considered an alternative model, which can explain the laboratory data with a significantly lower modulus ratio.

The alternative they proposed is the clay particle model. In this model, the clays exist as a cylindrical particle (of radius c) that is attached tangentially to the pore wall (Figure 13). Because it is not mechanically coupled to the quartzo-feldspathic grain shell, the clays are shielded from any influence of the confining pressure applied to the external wall. For the clay particle model, Al-Wardy and Zimmerman (2004) obtained the following expression for the effective stress coefficient κ as a function of the modulus ratio γ, porosity ϕ, and volumetric clay fraction f_c:

$$\kappa=\frac{2+\phi+(1-\phi)f_c}{3}+\gamma(1-\phi)(1-f_c)\,g(\rho), \tag{7a}$$

where $g(\rho)$ is a function of the ratio ρ between the radii of the clay particle and pore conduit, which can be approximated analytically as

$$g(\rho)=0.0481\times\frac{\rho+9.048\rho^2-11.39\rho^3}{1-0.4331\rho-1.306\rho^2+0.5482\rho^3}. \tag{7b}$$

The ratio ρ can in turn be related to the porosity and clay fraction:

$$\rho=c/a=\sqrt{(1-\phi)f_c/[f_c+\phi(1-f_c)]}. \tag{7c}$$

Again, for mathematical convenience, we here follow Al-Wardy and Zimmerman (2004) to assume that clay particle and grain shell have identical Poisson's ratio of 0.25.

As illustrated in Figure 13, the clay particle model also predicts that the effective stress coefficient κ increases with increasing clay fraction and modulus contrast, as well as decreasing porosity. To bracket all the experimental data would take a modulus ratio γ significantly smaller than that necessary for the clay shell model (Figure 12), by at least a factor of two. In previous formulation of the clay shell and clay particle models, the existence of microcracks and where they may be located were not explicitly addressed. If we make the plausible assumption that the microcracks are embedded in the quartzo-feldspathic grains, then their shear moduli (and the corresponding modulus ratios γ) would

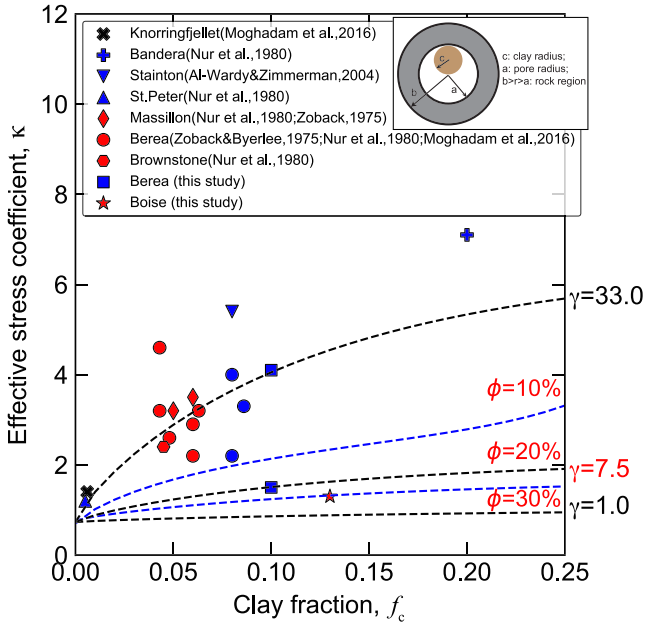

Figure 13. Effective stress coefficient as a function of clay fraction for different porosities and shear modulus ratio using the clay particle model. The points are data from this study and from the literature (see Table 2), and the black line refers to clay-particle model using the different ratio between rock and clay stiffness at the fixed porosity of 20%, the blue dash lines refer to clay-particle model using the different porosities of 10%, 20%, and 30% at the constant shear ratio of 7.5 with the Poisson ratio of rock and clay taken as 0.25.

increase with crack closure in the transition from stage I to II, and in either model the effective stress coefficient κ is predicted to increase (Figures 12 and 13), in agreement with our laboratory observations (Figure 4). Notwithstanding the better agreement with experimental observations, the clay particle model has the shortcoming as noted by Al-Wardy and Zimmerman (2004) that the inferred values of shear modulus ratio γ are somewhat higher than what one would predict from rock physics measurements for clays and crustal minerals, although there remain uncertainties on what data are pertinent and what constitutes a realistic approach to estimate the ratio.

The two models have quite different predictions regarding the effective stress coefficient β for pore volume change. The clay shell model assumes that the permeability and pore volume change both depend solely on the radius a, and accordingly their effective stress coefficients are predicted to be identical, given by $\kappa=\beta=-\left(\frac{\partial a}{\partial P_P}\right)/\left(\frac{\partial a}{\partial P_C}\right)$. Berryman (1992) has pointed out that this is speculative, and indeed recent experiments conducted by Wang et al. (2018) and Meng et al. (2019) on limestones showed that the predicted equality is consistently violated, such that the value of κ can be significantly greater than that of β.

For the clay particle model, we show in Appendix C that the effective stress coefficient for pore volume change is given by

$$\beta=\frac{2+\phi+(1-\phi)f_c}{3}+\frac{\gamma(1-\phi)(1-f_c)}{3}\rho^2. \tag{8a}$$

Given our measurements of the coefficient β (Figure 5), the above constrains values of γ to be about 4.3 and 3.5 for Boise and Berea sandstones, respectively. However, with reference to 7a, these γ values would imply that κ is just slightly greater than 1, in discrepancy with our measured values which are significantly larger ranging up to 4.5 (Figure 5). The discrepancy can be illustrated alternatively by subtracting 8a from 7a to arrive at

$$\kappa-\beta=\gamma(1-\phi)(1-f_c)\left[g(\rho)-\frac{\rho^2}{3}\right]. \tag{8b}$$

Unlike the clay shell model, the coefficient κ is predicted to always exceed β in the clay particle model, with the difference $\kappa-\beta$ increasing linearly with modulus contrast γ. As shown in Figure 14, for the porosity and clay fraction values of Berea and Boise sandstones 8b would imply $(\kappa-\beta)/\gamma$ to be about 0.02 and 0.03 for Boise and Berea sandstones, respectively. Given that measured values of $\kappa-\beta$ are in the ranges of 0.2–2.0 and 0.4–3.5 (Figure 4), this implies that γ has very large values up to 100 and 117 for Boise and Berea sandstones, respectively. This contradicts the relatively low γ values inferred from measured values of β on the basis of 8a. The implication is therefore neither the clay shell model nor the clay particle model that is based on a single equivalent channel can furnish a consistent interpretation of the data for the two effective stress coefficients κ and β simultaneously, and to resolve the discrepancy. It is necessary to consider a model that has more than one single channel.

4.5. A Dual Equivalent-Channel Model

In the clay particle and clay shell models, microscopic inhomogeneity derives from distinct mechanical responses of the clays and quartzo-feldspathic grains located in a single equivalent channel. In this sense, spatial heterogeneity is absent in the models. To introduce an element of spatial heterogeneity, we next consider a dual equivalent-channel model made up of two channels hydraulically connected in series (Figure 15). One of the equivalent channels corresponds to a clay-free porous constituent, and the other a clayey porous

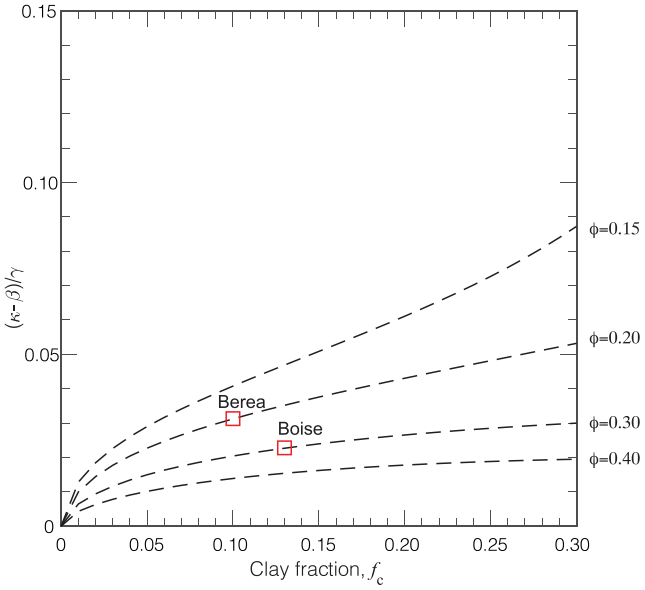

Figure 14. The ratio $(\kappa - \beta)/\gamma$ between the difference of the two effective stress coefficients for permeability and pore volume change and the shear modulus ratio is plotted as a function of clay fraction for different porosities in the clay particle model. Porosities and clay fractions of Berea and Boise sandstones are marked.

constituent. For mathematical convenience, we will consider a 2-dimensional model, with the geometry of the clayey channel given by the clay shell model (Figure 12). Similarly, the clay-free channel has a geometry similar to the clay shell model, except that the clay shell has zero thickness so that the radii $a = c$.

Effective stress coefficients for permeability for the clay-free and clayey channels are denoted by $\kappa'$and κ'', respectively, and the corresponding effective stress coefficients for pore volume change are denoted by β' and β'', respectively. Since the two equivalent channels are in series, if the permeabilities of the clay-free and clayey channels are denoted by $k'$and k'', then the effective permeability k of the dual system is given by

$$\frac{1}{k}=\frac{1}{k'}+\frac{1}{k''}. \tag{9a}$$

If the pore volumes taken up by the clay-free and clayey channels are denoted by $V_v^{'}$ and $V_v^{''}$, then the total pore volume in the dual system is given by

$$V_v=V_v^{'}+V_v^{''}. \tag{9b}$$

We will focus on the case with $k' \gg k''$, such that the flow is limited by the relatively impermeable clayey channel and the permeability of the dual system can be approximated as $k \approx k''$ according to 9a. This in turn implies that the interplay of confining and pore pressures on the permeability would be controlled by the effective stress behavior of the clayey channel, and therefore the effective stress coefficient of the dual system can also be approximated as

$$\kappa \approx \kappa''. \tag{10}$$

According to 9b a pore volume δV_v comprises two components $\delta V_v^{'}$ and $\delta V_v^{''}$, and because the local effective stress coefficients for pore volume change in the clay-free and clayey channels are given by β' and β'', respectively, the total pore volume change in response to a change δP_C in confining pressure and δP_p in pore pressure is given by

$$\delta V_v=\frac{\partial V_v^{'}}{\partial P_C}(\delta P_C-\beta'\delta P_P)+\frac{\partial V_v^{''}}{\partial P_C}(\delta P_C-\beta''\delta P_P). \tag{11a}$$

If the distribution of pore volume between the two equivalent channels is characterized by the partition parameter A, such that $V_v^{'}=AV_v$ and $V_v^{''}=(1-A)V_v$, then the above equation becomes

$$\delta V_v=\frac{\partial V_v}{\partial P_C}(\delta P_C-[A\beta'+(1-A)\beta'']\delta P_P). \tag{11b}$$

This implies that the effective stress coefficient for volume change in the dual system is given by

$$\beta=A\beta'+(1-A)\beta''. \tag{12a}$$

Given that the two equivalent channels are both of the clay shell type, their local effective stress coefficients are equal ($\kappa' = \beta'$ and $\kappa'' = \beta''$), and we can rewrite the above as $\beta = A\kappa'+(1-A)\kappa''$. Furthermore, if the approximation 10 applies, then a linear relation exists between the two effective coefficients β and κ of the dual equivalent-channel system:

$$\beta=A\kappa'+(1-A)\kappa. \tag{12b}$$

To compare this theoretical prediction with our laboratory data, a major difficulty is to arrive at a realistic estimate of the effective stress coefficient $\kappa' = \beta'$ for a clay-free assemblage. For the clay shell

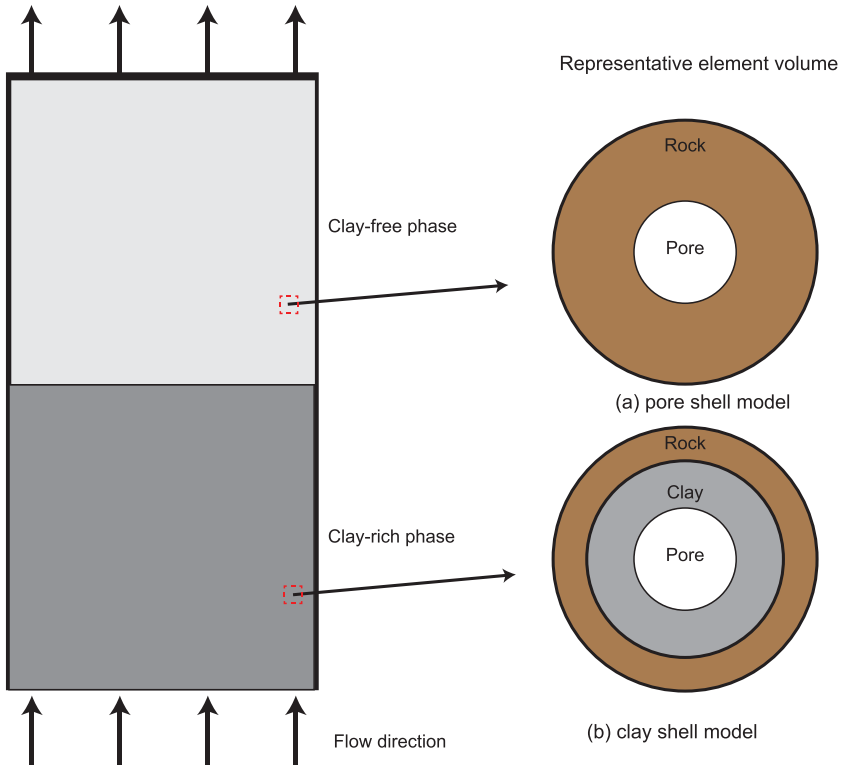

Figure 15. Schematic diagram of the dual-equivalent channel model.

model with zero thickness (Al-Wardy & Zimmerman, 2004), assuming a Poisson's ratio of 0.25, the effective stress coefficient for a clay-free channel is $\kappa' = \beta' = (2+\phi)/3$, equal to 0.73 and 0.77 for porosities of 20% and 30%, respectively. There are also two sets of pertinent laboratory data: David and Darot (1989) reported κ values between 0.60 and 0.75 for Fontainebleau sandstone, and Nur et al. (1980) reported values of 0.43 and 0.86 for two Al_2O_3 samples. Since all these experiments were at conditions with microcrack closure, they are more relevant to stage II of Berea sandstone and Boise sandstone under high confinement. For these experimental data, if we adopt an intermediate value of $\kappa' = 0.6$, then the linear relation 12b implies values of A between 0.91 and 0.95 for stage II of Berea sandstone (Figure 16a), and 0.84 for Boise sandstone at confining pressure of 28 MPa (marked using circle in Figure 16b).

For stage I of Berea sandstone and Boise sandstone under low confinement, we must take into account the presence of microcracks on the effective stress coefficients. Given the inequality $\alpha \leq \beta \leq \kappa \leq 1$ for a microscopically homogeneous assemblage (Berryman, 1992), and the experimental observations (Paterson & Wong, 2005) and theoretical prediction (Wong, 2017) that the Biot coefficient α increases with increasing crack density to approach an asymptotic limit of 1, one would expect both effective stress coefficients β and κ to also increase with increasing crack density. Indeed, Bernabe (1987) observed a systematic decrease of the coefficient κ in three crystalline rocks with crack closure under increasing confining pressure. This implies that we must adopt a higher value of $\kappa' > 0.6$ in 12b for comparison with data of a cracked rock. On the other hand, it seems unlikely for the partition parameter A to vary significantly between stage I and II in Berea sandstone. If we use the same A values for these two stages, then the laboratory data in stage I are intersected by the two lines corresponding to κ' value of 0.9. Similarly, a value of $\kappa' = 0.9$ is inferred for Boise sandstone at confining pressure of 22 MPa.

By introducing an element of spatial heterogeneity in the distribution of clays, the dual equivalent-channel model analyzed here provides an explanation for the two effective stress coefficients κ and β being not equal. The permeability of the dual system is controlled by that of the clayey channel, because the rate of flow is

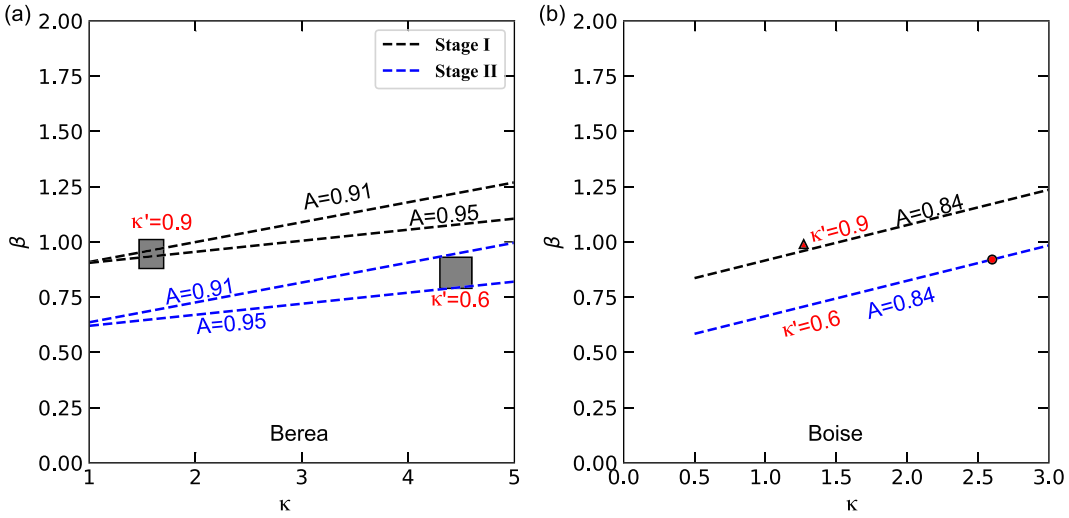

Figure 16. Effective stress coefficient β for pore volume change as a function of effective stress coefficient for permeability κ using the dual equivalent-channel model. (a) The gray box indicates the data ranges for Berea sample in stage I and stage II. These data can be bracketed by the theoretical predictions of dual-equivalent channel model for A between 0.91–0.95 using κ′ of 0.9 in stage I (black dashed lines) and 0.6 stage II (blue dashed lines). (b) The red triangle and circle indicate the coefficients for Boise sandstone at the confining pressures of 22 and 28 MPa, respectively. They can be theoretically predicted by dual equivalent-channel model for A with value of 0.84 using κ′ of 0.9 at the confining pressure of 22 MPa (black dashed line) and 0.6 at the confining pressure of 28 MPa (blue dashed line).

limited by the very low permeability of the clays embedded in the channel. Accordingly, the effective stress coefficient κ for permeability is also controlled by the clayey channel. In the clay particle and clay shell models, because only one equivalent channel is being considered, the local clay content in the channel is assumed to be identical to the global clay content determined from XRPD. However, in the dual equivalent-channel model the clays are localized only in a subset of the conduits (as indicated by the clay partition 1-*A*), and therefore the local clay content may be significantly higher than the global average, which implies that the enhancement of effective stress coefficient can then be interpreted using a much smaller modulus contrast γ (Figures 12 and 13).

The effective stress coefficient β for pore volume change is predicted to increase with the effective stress coefficient κ for permeability, in agreement with Berryman's (1992) model (Figure 11). According to 12b, because κ is greater than κ' of the nonclay assemblage, the coefficient κ is predicted to be always greater than β, in agreement with laboratory observations in regime II (Figure 10). The difference between the two coefficients hinges on the partitioning of pore volume between the nonclay and clayey channels, as characterized by the parameter *A*.

However, it should be emphasized that the dual equivalent-channel model is highly idealized and in particular the assumption is made that the two channels are in series and, for mathematical convenience, we focus here on the case $k' \gg k''$ such that the flow is limited by the relatively impermeable clayey channel. It is likely that the idealized model may fail to capture all relevant complexities of the flow field of a clayey sandstone. In sedimentary petrography, the spatial distribution of clay minerals in sandstones is often categorized into three conceptual scenarios: discrete particles of clay dispersed in the pore space, pore-lining rims of clay minerals, and pore-bridging clays (Blasingame, 2008; Howard, 1992; Neasham, 1977). These three scenarios are associated with progressive decrease of permeability; for the third scenario, data for the Rotliegende sandstones of the southern North Sea show that samples with fibrous illite filling the pores may have permeabilities lower than the first two categories by two orders of magnitude (Seemann, 1979). What we consider here corresponds to this end-member scenario with pore-bridging clays that limit the rate of fluid transport in the clayey sandstone.

Because of its idealized nature, there remain aspects of the model that are difficult to characterize. The connection between the partition parameter A and the spatial distribution of clays in the rock needs to be clarified by systematic microstructural investigations. The geometry of the pore space and mineralogy, as well as their spatial complexity, can all influence the grain-scale deformation and effective stress behavior. To advance beyond such a model of equivalent channels in an effective medium, it may be necessary to probe more deeply and integrate 3-D microstructural observations with voxel-based numerical simulations (Sun & Wong, 2018; Zhan et al., 2010).

5. Conclusion

The influence of confining and pore pressures on permeability and pore volume change, as manifested by the effective stress coefficients κ and β, was studied in two clayey sandstones over a broad range of confining and pore pressures. Because hydrostatic compression of a porous rock typically involves an initial nonlinear stage I of elastic crack closure and a subsequent linear stage II of pore deformation, we characterized the effective stress coefficients κ and β separately in these two stages. Our data show that the coefficients κ for permeability of both clayey sandstones are uniformly greater than 1, in agreement with previous studies. Furthermore, we observed values of κ during stage I to be significantly smaller than in stage II for Berea sandstone. For Boise sandstone, we were not able to conduct measurements separately in two stages, but our data indicate an increase of κ with increasing confinement and crack closure, also by a factor of >2. We obtained some of the first measurement of the effective stress coefficient for pore volume change in sandstone. Values of β for both clayey sandstones are uniformly less than 1, approaching to unity. Based on our new sandstone data, recent data on limestone, and some theoretical analyses, we proposed to define in the β-κ space two fundamentally different regimes for the effective stress behavior: Regime I for microscopically homogenous rocks with $\beta \leq \kappa \leq 1$, and Regime II for microscopically inhomogeneous rocks with $\kappa > 1$. The latter regime may be partitioned further into a Regime IIA represented by clayey sandstones with $\beta \leq 1$ and Regime IIB represented by limestones with dual-porosity with $\beta > 1$. We confronted our data to the existing models for the effective stress behavior of inhomogeneous rock. The clay shell model assumes that the effective stress coefficient for permeability is equal to the effective stress coefficient for pore volume change, which is not what we observed. The clay particle model predicts the effective stress coefficient κ to be greater than β in qualitative agreement with experimental data, but it fails to quantitatively provide a consistent interpretation of both coefficients. Moreover, Berryman's model lacks any realistic assumption about pore space geometry. We therefore extended the clay shell model into a new dual equivalent-channel model considering the microscopical geometry to differentiate the coefficients κ and β. This new model can reasonably explain the micromechanics of effective stress behavior at the different deformation stages, providing new insight into the influence of pore geometry and mechanical contrast on the effective stress behavior for different physical properties of porous rocks.

Appendix A: Biot's Coefficient for a Clayey Sandstone

Nur and Byerlee (1971) rigorously derived a relation for Biot's effective stress coefficient α for bulk strain in terms of the bulk moduli K and K_s of the porous rock and solid grains, respectively:

$$\alpha = 1 - \frac{K}{K_s} = 1 - \frac{\beta_s}{\beta_V}. \tag{A1}$$

The corresponding compressibilities are denoted by β_V and β_s, respectively. Although the rock is assumed to be microscopically homogeneous in their derivation, Berryman (1992) argued that A1 is still a valid approximation for a microscopically inhomogeneous assemblage in the form of a clayey sandstone. Indeed, Hart and Wang (1995) measured the Biot coefficient and bulk moduli, and they demonstrated the validity of this expression for Berea sandstone. Accordingly, we will use the relation A1 to infer the coefficient α from hydrostatic compression experiment.

For intrinsic compressibility of the solid grains, we adopted values for Berea sandstone (0.0253/GPa) and Boise sandstone (0.0257/GPa) determined by Wong et al. (1997) using the Voigt-Reuss-Hill of the mineral elastic constants. The effective solid bulk modulus K_s is the inverse of the intrinsic compressibility β_s,

assuming for Berea sandstone and for Boise sandstone that we follow the estimation from Wong et al. (1997). For the bulk compressibility β_V, we use the following equation that connects it with the porosity ϕ and pore compressibility β_ϕ (Walsh, 1965):

$$\beta_V = \beta_\phi \cdot \phi + \beta_s. \tag{A2}$$

The porosity was taken to be 20% and 30% for Berea and Boise sandstones, respectively. For the pore compressibility, we used the values obtained from linear regression of the data presented in Figure 7. On substituting into A1, based the effective stress coefficients α for strain were inferred to be 0.80, 0.65, and 0.84 for stage I and stage II for Berea sandstone, and stage I&II for Boise sandstone, respectively. These values are all less than unity and comparable in magnitude to published data (Paterson & Wong, 2005). For Berea sandstone, the inferred α value in stage I is larger than that in stage II.

Appendix B: Relevant Results of the Clay Shell Model

Al-Wardy and Zimmerman (2004) made a rigorous derivation for calculating the effective stress coefficient κ in clay shell model quantitatively:

$$\kappa = \frac{A_{1p}a^2 + B_{1p}}{A_{1c}a^2 + B_{1c}}, \tag{B1}$$

Where

$$A_{1p} = \frac{2b^4 G_c G_r}{\Delta}\left[\varnothing\left(f_c(1-\phi)+\phi+\frac{1}{1-2\nu_r}\right)+\gamma\phi\left(f_c(1-\phi)+\phi-1\right)\left(\frac{1}{1-2\nu_r}\right)\right], \tag{B2}$$

$$A_{1c} = -\frac{2b^4 G_c G_r}{\Delta}\left[\left(f_c(1-\phi)+\phi+\frac{1}{1-2\nu_r}\right)+\left(f_c(1-\phi)+\phi-1\right)\left(\frac{1}{1-2\nu_r}\right)\right], \tag{B3}$$

$$B_{1p} = \left(\frac{1}{1-2\nu_c}\right)a^2 A_{1p} + \frac{a^2}{2G_c}, \tag{B4}$$

$$B_{1c} = \left(\frac{1}{1-2\nu_c}\right)a^2 A_{1c}, \tag{B5}$$

$$\Delta = 4b^4 G_c{}^2 G_r\left\{\left(\frac{1}{1-2\nu_c}\right)\left[\left(f_c(1-\phi)+\phi\right)+\left(\frac{1}{1-2\nu_r}\right)\right]\left(f_c(1-\phi)\right)-\left(\frac{1}{1-2\nu_r}\right)\left[\gamma\left(f_c(1-\phi)+\phi\right)+\left(\frac{1}{1-2\nu_r}\right)\gamma\phi\right]\left(f_c(1-\phi)+\phi-1\right)\right\}, \tag{B6}$$

where $\gamma = \frac{G_r}{G_c}$, $\frac{\lambda}{G} = \frac{2\nu}{1-2\nu}$. ϕ is porosity; f_c is the volumetric fraction of clay content; a is pore radius in the clay shell model; the moduli will be $\{\lambda_c, G_c\}$ in the clay region, $a < r < c$; and the moduli are $\{\lambda_r, G_r\}$ in the rock region, $c < r < b$. ν is Poisson's ratio. According to the expression of B_{1p} and B_{1c}, we can simplify the expression of κ,

$$\kappa = \frac{2\left(\frac{1-\nu_c}{1-2\nu_c}\right)A_{1p} + \frac{1}{2G_c}}{2\left(\frac{1-\nu_c}{1-2\nu_c}\right)A_{1c}}. \tag{B7}$$

The general expression of the effective stress coefficient for permeability can be obtained by substituting Equations B2, B3, and B6 into this Equation B7. Then

$$\kappa = \frac{\left[\left(f_c(1-\phi)+\phi\right)+\left(\frac{1}{1-2\nu_r}\right)\right]\left[\left(f_c(1-\phi)+\phi\right)\left(\frac{1}{1-2\nu_r}\right)+\phi\right]+\gamma\left(f_c(1-\phi)+\phi-1\right)\left(\frac{1}{1-2\nu_r}\right)\left[\phi\left(\frac{2\nu_c}{1-2\nu_c}-\frac{2\nu_r}{1-2\nu_r}\right)-f_c(1-\phi)\right]}{4\left[f_c(1-\phi)+\phi\right]\left(\frac{1-\nu_r}{1-2\nu_r}\right)\left(\frac{1-\nu_c}{1-2\nu_c}\right)}. \tag{B8}$$

If we assume the Poisson's ratio of both clay and rock region is 0.25, then we can get

$$\kappa=\frac{[f_c(1-\phi)+\phi+2][2f_c(1-\phi)+3\phi]+2\gamma f_c(1-f_c)(1-\phi)^2}{9[f_c(1-\phi)+\phi]}. \tag{B9}$$

Appendix C: Relevant Results of the Clay Particle Model

In the clay particle model (Figure 13), the clays exist as a cylindrical particle (of radius c) attached tangentially to the pore wall (of radius a). As analyzed by Al-Wardy and Zimmerman (2004), the particle is mechanically decoupled from the stress field related to the applied confining pressure, and it deforms in response to only the pore pressure. Therefore, its radius c is independent of P_c and a function of P_p only. Accordingly, the effective stress coefficient for pore volume (V_P) change is simply given by

$$\beta=-\left[\frac{\frac{\partial V_P}{\partial a}\frac{\partial a}{\partial P_P}+\frac{\partial V_P}{\partial c}\frac{\partial c}{\partial P_P}}{\frac{\partial V_P}{\partial a}\frac{\partial a}{\partial P_C}}\right]=-\left(\frac{\frac{\partial a}{\partial P_P}}{\frac{\partial a}{\partial P_C}}\right)-\left(\frac{\frac{\partial V_P}{\partial c}\frac{\partial c}{\partial P_P}}{\frac{\partial V_P}{\partial a}\frac{\partial a}{\partial P_C}}\right). \tag{C1}$$

Following Al-Wardy and Zimmerman (2004), the first term above can be written as

$$-\left(\frac{\frac{\partial a}{\partial P_P}}{\frac{\partial a}{\partial P_C}}\right)=\frac{\lambda_r+G_r(1+\phi')}{\lambda_r+2G_r}, \tag{C2}$$

where $\phi'=\frac{a^2}{b^2}=\phi+(1-\phi)f_c$, and the two derivatives in the second term are given by

$$\frac{\partial c}{\partial P_P}=-\frac{c}{2(\lambda_c+G_c)}, \tag{C3}$$

$$\frac{\partial a}{\partial P_C}=-\frac{a}{2(1-\phi')}\frac{\lambda_r+2G_r}{G_r(\lambda_r+G_r)}. \tag{C4}$$

Because the pore volume per unit length is $V_P=\pi(a^2-c^2)$, using expressions from C3 and C4 the second term in C1 can now be simplified as

$$-\frac{\frac{\partial V_P}{\partial c}\frac{\partial c}{\partial P_P}}{\frac{\partial V_P}{\partial a}\frac{\partial a}{\partial P_C}}=\left(\frac{c}{a}\right)^2\left(\frac{1-\phi'}{\lambda_c+G_c}\right)\left[\frac{G_r(\lambda_r+G_r)}{\lambda_r+2G_r}\right]. \tag{C5}$$

Adding C2 and C5 and then substituting into C1, we obtain the effective stress coefficient for pore volume change as

$$\beta=\frac{\lambda_r+G_r(1+\phi')}{\lambda_r+2G_r}+\left(\frac{c}{a}\right)^2\frac{(1-\phi')}{(\lambda_c+G_c)}\frac{G_r(\lambda_r+G_r)}{\lambda_r+2G_r}. \tag{C6}$$

Using 7c to relate the ratio c/a to the porosity and clay fraction, and assuming the Poisson's ratio of clay and rock regions are both 0.25, we arrive at Equation 8a in the main text.

Acknowledgments

We are grateful to the editors and two anonymous reviewers for their constructive comments and suggestions. This study was partially supported by funding from the Hong Kong Research Grants Council GRF14323916, the France-Hong Kong Collaborative Program Procore 30805PM and F-CUHK405/16, CNRS (PICS 07961), and NSFC/RGC Joint Research Scheme N_CUHK418/15. The first author was supported by the Impact Postdoctoral Fellowship Scheme of The Chinese University of Hong Kong. The data will be made available to the scientific community online (https://doi.pangaea.de/10.1594/PANGAEA.913507).

References

Al-Wardy, W., & Zimmerman, R. W. (2004). Effective stress law for the permeability of clay-rich sandstones. *Journal of Geophysical Research*, *109*, B04203. https://doi.org/10.01029/02003JB002836

Baud, P., Reuschlé, T., Ji, Y., Cheung, C. S. N., & Wong, T.-F. (2015). Mechanical compaction and strain localization in Bleurswiller sandstone. *Journal of Geophysical Research: Solid Earth*, *120*, 6501–6522. https://doi.org/10.1002/2015JB012192

Bergmann, J., Friedel, P., & Kleeberg, R. (1998). BGMN—A new fundamental parameters based Rietveld program for laboratory X-ray sources, its use in quantitative analysis and structure investigations. *CPD Newsletter*, *20*(5).

Bernabe, Y. (1986). The effective pressure law for permeability in Chelmsford granite and Barre granite. *In International Journal of Rock Mechanics and Mining Sciences & Geomechanics Abstracts*, *23*(3), 267–275. https://doi.org/10.1016/0148-9062(86)90972-1

Bernabe, Y. (1987). The effective pressure law for permeability during pore pressure and confining pressure cycling of several crystalline rocks. *Journal of Geophysical Research*, *92*, 649–657. https://doi.org/10.1029/JB092iB01p00649

Berryman, J. G. (1992). Effective stress for transport properties of inhomogenous porous rock. *Journal of Geophysical Research*, *97*, 17,409–17,424. https://doi.org/10.1029/92JB01593

Berryman, J. G., & Milton, G. W. (1991). Exact results for generalized Gassmann's equations in composite porous media with two constituents. *Geophysics*, *56*(12), 1950–1960. https://doi.org/10.1190/1.1443006

Blasingame, T. A. (2008). The characteristic flow behavior of low-permeability reservoir systems. In SPE Unconventional Reservoirs Conference. *Society of Petroleum Engineers*. https://doi.org/10.2118/114168-MS

Brace, W. F. (1965). Some new measurements of linear compressibility of rocks. *Journal of Geophysical Research*, *70*(2), 391–398. https://doi.org/10.1029/JZ070i002p00391

Bredehoeft, J. D., & Norton, D. L. (Eds) (1990). *The Role of Fluids in Crustal Processes* (p. 170). Washington, D. C: National Academy Press.

Coyner, K. B. (1984). Effects of stress, pore pressure, and pore fluids on bulk strain, velocity, and permeability of rocks. (PhD), *Massachusetts Institute of Technology*, Cambridge.

David, C., & Darot, M. (1989). Permeability and conductivity of sandstones. *ISRM international symposium*. International Society for Rock Mechanics and Rock Engineering.

David, C., Wong, T. F., Zhu, W., & Zhang, J. (1994). Laboratory measurement of compaction-induced permeability change in porous rocks: Implications for the generation and maintenance of pore pressure excess in the crust. *Pure and Applied Geophysics*, *143*(1–3), 425–456.

Fatt, I. (1958). Compressibility of sandstones at low to moderate pressures. *AAPG Bulletin*, *42*(8), 1924–1957.

Ghabezloo, S., Sulem, J., Guédon, S., & Martineau, F. (2009). Effective stress law for the permeability of a limestone. *International Journal of Rock Mechanics and Mining Sciences*, *46*(2), 297–306. https://doi.org/10.1016/j.ijrmms.2008.05.006

Hart, D. J., & Wang, H. F. (1995). Laboratory measurements of a complete set of poroelastic moduli of Berea sandstone and Indiana limestone. *Journal of Geophysical Research*, *100*, 17,741–17,751. https://doi.org/10.1029/95JB01242

Heap, M. J., Kushnir, A. R., Gilg, H. A., Wadsworth, F. B., Reuschlé, T., & Baud, P. (2017). Microstructural and petrophysical properties of the Permo-Triassic sandstones (Buntsandstein) from the Soultz-sous-Forêts geothermal site (France). *Geothermal Energy*, *5*(1), 26. https://doi.org/10.1186/s40517-017-0085-9

Heller, R., Vermylen, J., & Zoback, M. (2014). Experimental investigation of matrix permeability of gas shales. *AAPG Bulletin*, *98*, 975–995. https://doi.org/10.1306/09231313023

Howard, J. J. (1992). Influence of authigenic clay minerals on permeability. In *Origin, Diagenesis, and Petrophysics of Clay Minerals in Sandstones*, *Special Publications* (Vol. 47, 257–264). Society of Sedimentary Geology. https://doi.org/10.2110/pec.92.47.0257

Ingebritsen, S. E., & Sanford, W. E. (2006). *Groundwater in Geologic Processes* (p. 341). New York: Cambridge University Press.

Jaeger, J. C., Cook, N. G. W., & Zimmerman, R. W. (2007). *Fundamentals of rock Mechanics* (4th ed.). Oxford: Blackwell. https://doi.org/10.1017/CBO9780511735349

Kranz, R. L., Frankel, A. D., Engelder, T., & Scholz, C. H. (1979). The permeability of whole and jointed Barre granite. *In International Journal of Rock Mechanics and Mining Sciences & Geomechanics Abstracts*, *16*(4), 225–234. https://doi.org/10.1016/0148-9062(79)91197-5

Kwon, O., Kronenberg, A. K., Gangi, A. F., & Johnson, B. (2001). Permeability of Wilcox shale and its effective pressure law. *Journal of Geophysical Research*, *106*(B9), 19,339–19,353. https://doi.org/10.1029/2001JB000273

Mavko, G., Mukerji, T., & Dvorkin, J. (2009). *The rock physics handbook* (Second ed.). Cambridge University Press.

Meng, F., Baud, P., Ge, H., & Wong, T. F. (2019). The effect of stress on limestone permeability and effective stress behavior of damaged samples. *Journal of Geophysical Research: Solid Earth*, *124*, 376–399. https://doi.org/10.1029/2018JB016526

Moghadam, J. N., Mondol, N. H., Aagaard, P., & Hellevang, H. (2016). Effective stress law for the permeability of clay-bearing sandstones by the Modified Clay Shell model. *Greenhouse Gases: Science and Technology*, *6*(6), 752–774. https://doi.org/10.1002/ghg.1612

Neasham, J. W. (1977). The morphology of dispersed clay in sandstone reservoirs and its effect on sandstone shaliness, pore space and fluid flow properties. *Society of Petroleum Engineers SPE Paper* 6858, https://doi.org/10.2118/6858-MS

Nur, A., & Byerlee, J. (1971). An exact effective stress law for elastic deformation of rock with fluids. *Journal of Geophysical Research*, *76*(26), 6414–6419. https://doi.org/10.1029/JB076i026p06414

Nur, A. M., Walls, J. D., Winkler, K., & DeVilbiss, J. (1980). Effects of fluid saturation on waves in porous rock and relations to hydraulic permeability. *Society of Petroleum Engineers Journal*, *20*(06), 450–458. https://doi.org/10.2118/8235-PA

Paterson, M. S., & Wong, T. F. (2005). *Experimental rock deformation-the brittle field*. Springer Science & Business Media. https://doi.org/10.1007/b137431

Seemann, U. (1979). Diagenetically formed interstitial clay minerals as a factor in Rotliegend sandstone reservoir quality in the Dutch section of the North Sea. *Journal of Petroleum Geology*, *1*, 55–62. https://doi.org/10.1111/j.1747-5457.1979.tb00619.x

Sun, W., & Wong, T. F. (2018). Prediction of permeability and formation factor of sandstone with hybrid lattice Boltzmann/finite element simulation on microtomographic images. *International Journal of Rock Mechanics and Mining Sciences*, *106*, 269–277. https://doi.org/10.1016/j.ijrmms.2018.04.020

Terzaghi, K. (1936). The shearing resistance of saturated soils, *Proc. 1st Int. Conf. Soil Mech*. (pp. 54–56).

Vajdova, V., Baud, P., & Wong, T.-F. (2004). Compaction, dilatancy and failure in porous carbonate rocks. *Journal of Geophysical Research*, *109*, B05204. https://doi.org/10.1029/2003JB002508

Walls, J., & Nur, A. (1979). Pore pressure and confining pressure dependence of permeability in sandstone, in *Proceedings of the 7th Formation Evaluation Symposium of the Canadian Well Logging Society*, paper O, Can. Well Logging Soc., Alberta, Calgary.

Walsh, J. B. (1965). The effect of cracks on the compressibility of rock. *Journal of Geophysical Research*, *70*(2), 381–389. https://doi.org/10.1029/JZ070i002p00381

Walsh, J. B. (1981). Effect of pore pressure and confining pressure on fracture permeability. *International Journal of Rock Mechanics and Mining Sciences*, *18*(5), 429–435. https://doi.org/10.1016/0148-9062(81)90006-1

Wang, Y., Meng, F., Wang, X., Baud, P., & Wong, T. F. (2018). Effective stress law for the permeability and deformation of four porous limestones. *Journal of Geophysical Research: Solid Earth*, *123*, 4707–4729. https://doi.org/10.1029/2018JB015539

Wong, T. F. (2017). Anisotropic poroelasticity in a rock with cracks. *Journal of Geophysical Research: Solid Earth*, *122*, 7739–7753. https://doi.org/10.1002/2017JB014315

Wong, T. F., David, C., & Zhu, W. (1997). The transition from brittle faulting to cataclastic flow in porous sandstones: Mechanical deformation. *Journal of Geophysical Research*, *102*(B2), 3009–3025. https://doi.org/10.1029/96JB03281

Zhan, X., Schwartz, L. M., Toksöz, M. N., Smith, W. C., & Morgan, F. D. (2010). Pore-scale modeling of electrical and fluid transport in Berea sandstone. *Geophysics*, *75*(5), F135–F142. https://doi.org/10.1190/1.3463704

Zimmerman, R. W., Somerton, W. H., & King, M. S. (1986). Compressibility of porous rocks. *Journal of Geophysical Research*, *91*, 12,765–12,777. https://doi.org/10.1029/JB091iB12p12765

Zoback, M. D. (1975). High pressure deformation and fluid flow in sandstone, granite, and granular materials, Ph.D. thesis, Stanford Univ., Stanford, Calif.

Zoback, M. D. (2007). *Reservoir Geomechanics*. Cambridge: Cambridge University Press.

Zoback, M. D., & Byerlee, J. D. (1975). Permeability and effective stress: Geologic notes. *AAPG Bulletin*, *59*(1), 154–158. https://doi.org/10.1306/83D91C40-16C7-11D7-8645000102C1865D